Icarus 257 (2015) 417–427

Contents lists available at ScienceDirect

Icarus

journal homepage: www.elsevier.com/locate/icarus

Chlorine on the surface of Mercury: MESSENGER gamma-ray measurements and implications for the planet's formation and evolution

Larry G. Evans [a,*], Patrick N. Peplowski [b], Francis M. McCubbin [c], Timothy J. McCoy [d], Larry R. Nittler [e], Mikhail Yu. Zolotov [f], Denton S. Ebel [g], David J. Lawrence [b], Richard D. Starr [h], Shoshana Z. Weider [e], Sean C. Solomon [e,i]

[a] Computer Sciences Corporation, Lanham-Seabrook, MD 20706, USA
[b] The Johns Hopkins University Applied Physics Laboratory, Laurel, MD 20723, USA
[c] Institute of Meteoritics, Department of Earth and Planetary Sciences, University of New Mexico, Albuquerque, NM 87131, USA
[d] National Museum of Natural History, Smithsonian Institution, Washington, DC 20013, USA
[e] Department of Terrestrial Magnetism, Carnegie Institution of Washington, Washington, DC 20015, USA
[f] School of Earth and Space Exploration, Arizona State University, Tempe, AZ 85287, USA
[g] Department of Earth and Planetary Sciences, American Museum of Natural History, New York, NY 10024, USA
[h] Physics Department, Catholic University of America, Washington, DC 20064, USA
[i] Lamont-Doherty Earth Observatory, Columbia University, Palisades, NY 10964, USA

ARTICLE INFO

Article history:
Received 8 January 2015
Revised 29 April 2015
Accepted 29 April 2015
Available online 7 May 2015

Keywords:
Mercury, surface
Gamma-ray spectroscopy
Geological processes
Planetary formation

ABSTRACT

Orbital measurements obtained by the MESSENGER Gamma-Ray Spectrometer have been analyzed to determine the surface abundance of chlorine in Mercury's northern hemisphere. The derived Cl/Si mass ratio is 0.0057 ± 0.001, which for an assumed Si abundance of 24.6 wt% corresponds to 0.14 ± 0.03 wt% Cl. The abundance of Cl is a factor of 2.9 ± 1.3 higher in the north polar region (>80°N) than at latitudes 0–60°N, a latitudinal variation similar to that observed for Na. Our reported Cl abundances are consistent with measured bulk concentrations of neutron-absorbing elements on Mercury, particularly those observed at high northern latitudes. The Cl/K ratio on Mercury is chondritic, indicating a limited impact history akin to that of Mars, which accreted rapidly. Hypotheses for the origin of Mercury's high metal-to-silicate ratio must be able to reproduce Mercury's observed elemental abundances, including Cl. Chlorine is also an important magmatic volatile, and its elevated abundance in the northern polar region of Mercury indicates that it could have played a role in the production, ascent, and eruption of flood volcanic material in this region. We have identified several candidate primary mineralogical hosts for Cl on Mercury, including the halide minerals lawrencite ($FeCl_2$), sylvite (KCl), and halite (NaCl), as well as Cl-bearing alkali sulfides. Amphiboles, micas, apatite, and aqueously deposited halides, in contrast, may be ruled out as mineralogical hosts of Cl on Mercury.

1. Introduction

The MErcury Surface, Space ENvironment, GEochemistry, and Ranging (MESSENGER) spacecraft made three flybys of Mercury in 2008–2009 and began its primary orbital mission about the innermost planet on 18 March 2011. The spacecraft carries a suite of geochemical remote-sensing instruments (Solomon et al., 2007) that includes a Gamma-Ray and Neutron Spectrometer (GRNS). To date, gamma-ray measurements have been used to report the abundances of Na, Al, S, K, Ca, Fe, Th, and U in Mercury's near-surface materials (Evans et al., 2012; Peplowski et al., 2011, 2012b). Here, we extend the analysis of the gamma-ray dataset to determine the chlorine content of Mercury's surface for the first time, though an upper limit derived from measurements by MESSENGER's X-Ray Spectrometer was given by Nittler et al. (2011).

The abundances of volatile elements on a planetary surface are important indicators of endogenic and exogenic processes. This statement is particularly true for Mercury, for which several planetary formation scenarios predict depletion in the bulk abundances of volatile elements relative to the other terrestrial planetary bodies (Taylor and Scott, 2003; Taylor and McLennan, 2008). Previous MESSENGER measurements have shown that Mercury's surface is not depleted in the moderately volatile elements S, K, and Na

* Corresponding author.
E-mail address: Larry.G.Evans@nasa.gov (L.G. Evans).

http://dx.doi.org/10.1016/j.icarus.2015.04.039
0019-1035/

(Nittler et al., 2011; Peplowski et al., 2011; Evans et al., 2012) relative to the surfaces of the Moon and asteroid Vesta. Mercury's surface K/Th ratio is comparable to that of Earth and Mars (Peplowski et al., 2011; McCubbin et al., 2012). This result has led to rejection or at least reformulation of several of the formation mechanisms for the innermost planet (Peplowski et al., 2011).

The element chlorine is more susceptible to loss during planetary accretion than S, K, and Na (Sharp and Draper, 2013), so it may provide an even more stringent constraint on Mercury's formation and thermal evolution than the other volatile elements. Furthermore, Cl is an important magmatic volatile on Earth and Mars (Webster et al., 1999; Aiuppa et al., 2009; Filiberto and Treiman, 2009; McCubbin et al., 2013) and has been proposed to be an important volatile on Mercury (Zolotov, 2011). The determination of Mercury's Cl content is, therefore, a key component for understanding the nature of the widespread volcanism across that planet's surface (e.g., Head et al., 2008, 2011; Kerber et al., 2009; Goudge et al., 2014).

2. Gamma-ray spectroscopy

Gamma-ray spectroscopy is a method for measuring elemental abundances, including that of Cl, at a planet's surface from orbit. Gamma rays are emitted from the decay of long-lived radionuclides and from the interactions of galactic cosmic-rays (GCRs) with planetary materials. The interactions of secondary neutrons with atomic nuclei produce the majority of the emitted gamma rays. The primary modes of gamma-ray production are inelastic-scatter reactions with fast (>1 MeV) neutrons, neutron capture reactions with thermal (~0.02 eV) neutrons, and activation by both proton and neutron interactions. The gamma rays emitted by these interactions have characteristic energies that can be used to identify the nuclides involved, and their fluxes can be related to the abundance of that nuclide. Unlike other compositional remote-sensing measurements, e.g., X-ray fluorescence, that are sensitive only to the uppermost surface layer (<100 μm deep), orbital gamma-ray spectroscopy can measure elemental abundances in the top tens of centimeters beneath a planet's surface because of the high penetrability of MeV-energy photons (Evans et al., 1993). The mean free path of a 1 MeV photon is ~6 cm and that of an 8 MeV photon ~22 cm for a typical regolith density.

Deriving the surface composition from orbital gamma-ray measurements requires knowledge of the GCR flux incident on the surface, neutron production physics, gamma-ray production cross sections for both the inelastic and capture reactions of interest, the transport of gamma-rays from their production site to the instrument, and the detector response (e.g., Evans et al., 2012). Additional complications arise from gamma-ray emissions originating from nuclear interactions with the gamma-ray detector, materials surrounding the detector, and material in the rest of the spacecraft (Peplowski et al., 2012b). Fortunately, there is no detectable Cl background signal in MESSENGER GRS measurements, greatly simplifying the evaluation of Cl concentrations on Mercury.

The MESSENGER Gamma-Ray Spectrometer (GRS) consists of a high-purity Ge sensor that measures photons in the energy range from 60 keV to 9 MeV (Goldsten et al., 2007). The energy resolution was 4.8 keV at 1368 keV during Mercury orbital operations, which is an order of magnitude better than scintillator-based GRS systems and facilitated the identification of many elements, including Cl. Techniques for analyzing GRS data have been presented by Peplowski et al. (2011, 2012a) and Evans et al. (2012). To date, GRS data have provided abundances averaged over the northern hemisphere for Al, Ca, S, Fe (all normalized to Si), Th, and U, as well as spatially resolved measurements of Na and K. GRS gamma-ray data collection ended on 15 June 2012 following the expected end of life of the GRS cryocooler.

3. Gamma-ray dataset and analysis

The analysis in this paper makes use of GRS measurements from 24 March 2011 to 10 October 2011, a period that corresponds to the acquisition of those orbital measurements having the best resolution of energy. Because the sensitivity of orbiting gamma-ray experiments is limited by the photon flux from the surface of the planet, the large numbers of spectra acquired during this period were summed in order to obtain counting statistics sufficient for peak analysis. Methods used for spectral processing, including corrections for electronic gain related to temperature, followed those given by Peplowski et al. (2012a).

The GRS data processing system provides a means for accumulating summed spectra that satisfy a variety of criteria, including variable time intervals, latitude–longitude ranges, and altitude ranges. Because of MESSENGER's highly eccentric orbit, the choice of a summed spectrum to represent the planetary signal and one to represent the background is not straightforward. We take the background spectrum as an accumulation of measurements at altitudes greater than 12,000 km, where the solid angle subtended by the planet from the spacecraft is less than 0.06 sr (Peplowski et al., 2012a). At this distance, Mercury-originating signals are negligible and the GRS measurements are dominated by spacecraft-generated backgrounds. As in previous work (Evans et al., 2012), data were accumulated for different low-altitude cutoffs to determine the optimal altitude limits for the planetary signal detection. These included measurements for all altitudes less than 2000, 1500, and 1000 km. The choice of low-altitude cutoff represents a compromise; at lower altitudes the planetary signal-to-background ratio is higher, but there is less accumulation time and higher statistical uncertainty. An example of this trade-off was shown by Evans et al. (2012). The MESSENGER orbit and the altitude dependence of the GRS signal result in a latitude dependence of the spectra binned by altitude. For example, the latitude range for a 2000-km cutoff is primarily northward of 20°S and for 1000 km it is northward of 0°N (Peplowski et al., 2012a). The accumulation times for the spectra were 1.07×10^6 s, 8.40×10^5 s, and 5.96×10^5 s for the 2000-, 1500-, and 1000-km cutoff altitudes, respectively. The integration time for the high-altitude spectrum was 4.27×10^6 s. The GRS detector is generally pointed in the nadir direction during periapsis passes.

A comparison of the time-normalized summed spectra from high altitude and low altitude shows that most of the peaks in the low-altitude spectrum have corresponding peaks in the high-altitude spectrum (Fig. 1). Previous analyses provide guidance for removing these background signals (Peplowski et al., 2011, 2012b; Evans et al., 2012). Fortunately, there is no evidence for a Cl gamma-ray signature at high altitudes, facilitating a straightforward analysis of the low-altitude measurements. The methodology adopted here is similar to that for the Na analyses of Evans et al. (2012) and Peplowski et al. (2014), another element for which no spacecraft-originating signature was observed. We report our Cl abundance as a ratio to Si; the Si gamma-ray result required a background correction that followed the procedure of Evans et al. (2012).

The vast majority of counts in a GRS spectrum form a nearly smoothly varying continuum. This continuum has a number of sources, including gamma rays that are scattered in the planetary regolith and in the Ge detector, as well as bremsstrahlung from charged particles. The charged particles (GCRs) that interact in

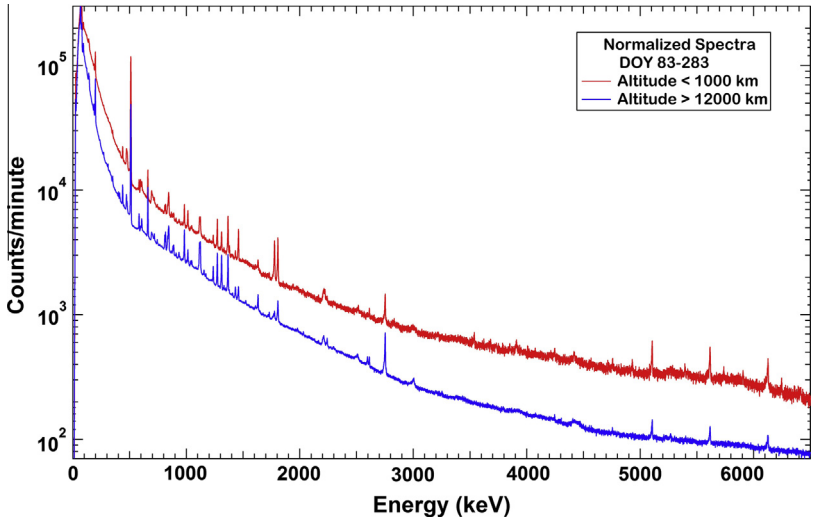

Fig. 1. Comparison of time-normalized low- and high-altitude GRS spectra summed over the period 24 March–10 October 2011. DOY denotes the day of the year in 2011.

the Ge detector and shield are vetoed with the GRS anti-coincidence logic (Goldsten et al., 2007), which significantly lowers the continuum, particularly at high (>4 MeV) energies. The continuum in the vicinity of a peak or a group of peaks is usually determined by fitting a slowly varying low-order polynomial to nearby portions of the spectrum that contain no discernible peaks. Superimposed on the continuum are a large number of discrete gamma-ray peaks (Fig. 1), most of which have a Gaussian shape with a low-energy tail caused by trapping effects and charge-collection losses in the detector. The tailing increases with the length of time spent in space because of radiation damage (Brückner et al., 1991). The tail is fit with an exponential that joins smoothly to the Gaussian shape. The width of these Gaussian-shaped peaks increases slowly and systematically with increasing energy. Calibration of the energy dependent spectral resolution can be used to help fit weak peaks (Evans et al., 2006). Gamma rays with energies greater than 1022 keV can interact in the detector by a process known as pair production, during which two 511 keV photons are created via electron-positron annihilation. One or both of these photons can escape the detector and produce gamma-ray peaks both at the full-energy peak minus 511 keV (termed the single-escape, or SE, peak) and at the full-energy peak minus 2×511 keV (termed the double-escape, or DE, peak).

Chlorine has a large cross-section for capture of thermal neutrons and emits a large number of emitted gamma rays after thermal neutron capture. In the analysis of Mars Odyssey GRS data, the Cl gamma rays at 1951, 1959, 6111, and 7790 keV were used to map Cl on the surface of Mars (Keller et al., 2006). Because of the lower detector efficiency of the MESSENGER GRS and the shorter accumulation time, the 7790 keV peak was not detectable, but the other peaks were observed. We also observed the two escape peaks for the 6111 keV gamma ray, which were used in the analysis. However, a complicating factor in this analysis was that the 6111 keV peak is approximately 511 keV lower than two other Cl peaks at 6620 and 6628 keV (analyzed as a single peak at 6624 keV). The SE and DE peaks of these chlorine gamma rays overlapped the 6111 keV peak and its SE peak, and this overlap had to be considered in the analysis. Additionally, the 6111 keV peak sits on the low-energy tail of the much larger 6129 keV oxygen photopeak, further complicating the analysis of that peak and also that of the escape peaks.

The low-energy Cl gamma rays were difficult to analyze from the low-altitude spectra with a 2000-km cutoff altitude, but the signal to background is larger for spectra collected with 1500-km and 1000-km cutoff altitudes, at a cost of higher statistical uncertainty. After a comparison of the results, the low-altitude spectrum with the 1000-km cutoff altitude was used for all the Cl analyses. In addition, the two 1951- and 1959-keV peaks were treated as one peak at 1955 keV. Fits to the low-energy Cl peak, for both the low-altitude and high-altitude spectra, are shown in Fig. 2.

An example of the fit to a high-energy Cl peak at 6111 keV is shown in Fig. 3. The large peak is the oxygen inelastic scatter peak at 6129 keV. To improve the statistics, after the analysis of the Cl photopeak and escape peaks, the counts were summed together. Before this analysis, the escape peak detection efficiency had not been characterized. We therefore used the oxygen peak at 6129 keV and a titanium peak at 6756 keV to estimate the escape peak detection efficiencies in the 6–7 MeV energy range. These results were then used to correct for the contributions to the higher-energy Cl peaks. The results for the Cl peaks are given in Table 1. Analysis of the high-altitude background spectrum collected far from the planet (Figs. 2b and 3b) indicates that there are no Cl background gamma rays arising from the spacecraft.

4. Forward calculations

The complexity of the process that produces planetary gamma rays from stable elements means that it is not possible to relate directly the measured peak intensities to elemental abundances on the surface of Mercury. Instead, for gamma rays produced by neutron interactions, peak intensities are compared with a forward-model calculation. The forward calculation depends on the flux and energy spectrum of incident cosmic rays, the assumed composition of the surface materials, and the properties of the gamma-ray detector. The production of neutrons was modeled with the Monte Carlo N-Particle eXtended (MCNPX) code for an influx of GCRs (Waters, 2002; McKinney et al., 2006). The surface composition used for the calculation was selected on the basis of results from laboratory modeling, MESSENGER X-Ray Spectrometer (XRS) measurements of major elements on Mercury (Nittler et al., 2011), GRS measurements of radioactive element abundances (Peplowski et al., 2011), and Neutron Spectrometer (NS) measurements (Lawrence et al., 2010). Details of the forward modeling used for MESSENGER GRS analyses were given by Evans et al. (2012). Note that the elements that have the largest effect on the neutron spectral and spatial distributions are hydrogen, elements of high atomic mass (e.g., Ca, Ti, Fe), and

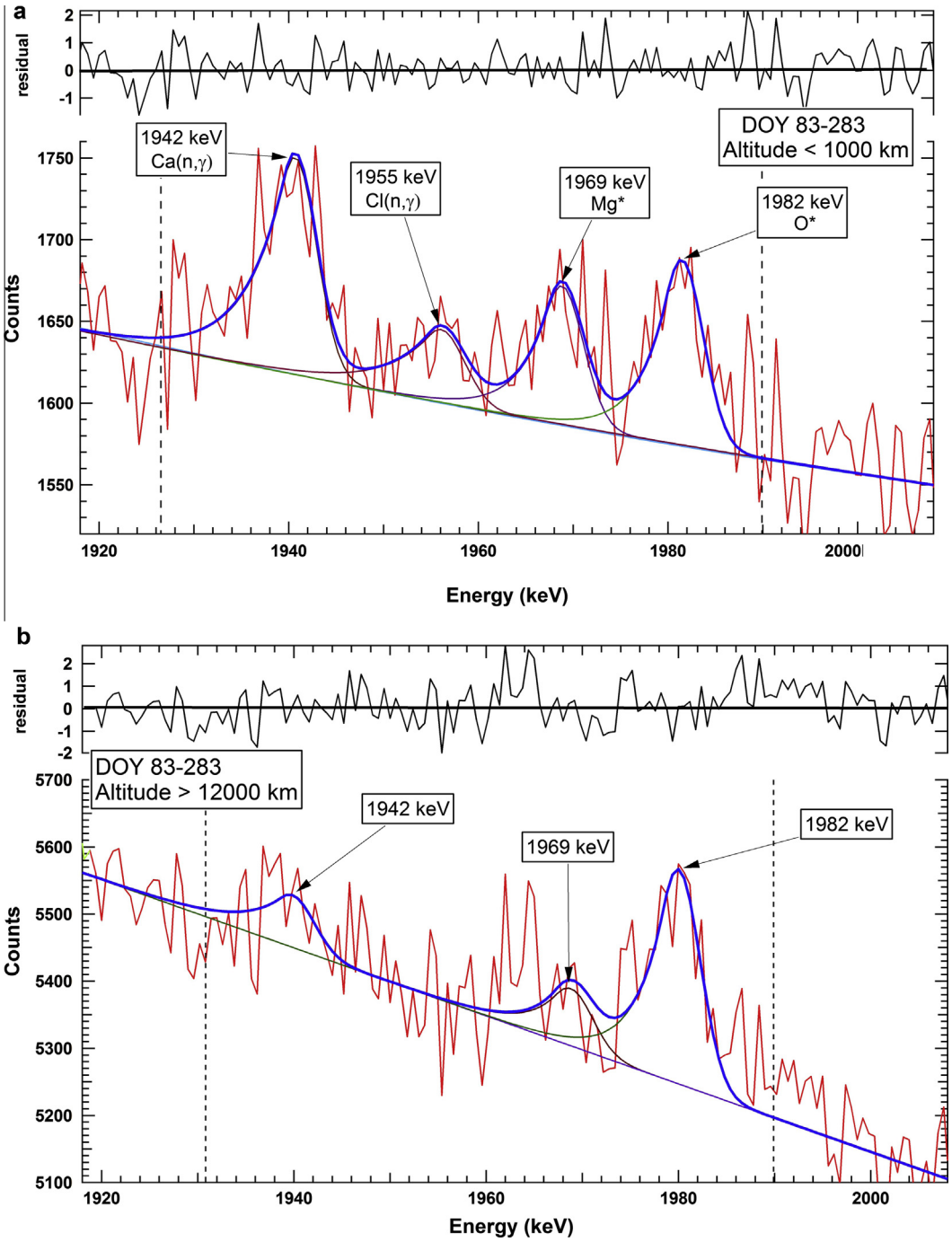

Fig. 2. Fits to spectral peaks in the energy range of the 1955-keV Cl peak. (a) Low-altitude spectrum; and (b) high-altitude spectrum. The other peaks in the spectra are from calcium (1942 keV), magnesium activation (Mg*, 1969 keV), and oxygen activation (O*, 1982 keV). Red curves show the measured spectrum, brown and green curves show the fits to each peak, and the thick blue curves show the sum of the individual peaks determined from the fits to the measurements. Vertical dashed lines denote the limits of the fitting region, and the black curves at the top of each panel, labeled residual, show the differences between the fit and the measurement in units of standard deviation. The accumulation times for the low-altitude and high-altitude spectra were 5.96×10^5 s, and 4.27×10^6 s, respectively. (For interpretation of the references to color in this figure legend, the reader is referred to the web version of this article.)

elements with large thermal neutron cross-sections, such as Cl and Mn. We discuss the contribution of Cl to neutron variability on Mercury in Section 5.

For each individual measurement in a spectral sum, the forward model includes calculations of the expected gamma-ray flux for the assumed surface composition. The abundance of a given element for that spectral sum is then determined by adjusting the model abundance by the ratio of the observed counts (minus any background) to the modeled counts for a particular gamma-ray peak. For elements with multiple gamma-ray lines, a mean is calculated (weighted by the inverse square of the uncertainties for the individual results). The absolute GCR flux varies with time and is not well characterized, so the results of GRS analyses are often presented as elemental ratios to remove the systematic variability of the GCR flux (Boynton et al., 2007). For Mars Odyssey gamma-ray measurements, the elemental concentrations were normalized to Si, which was specified to have a value of 20.95 wt% on the basis of in-situ analysis from Mars Pathfinder

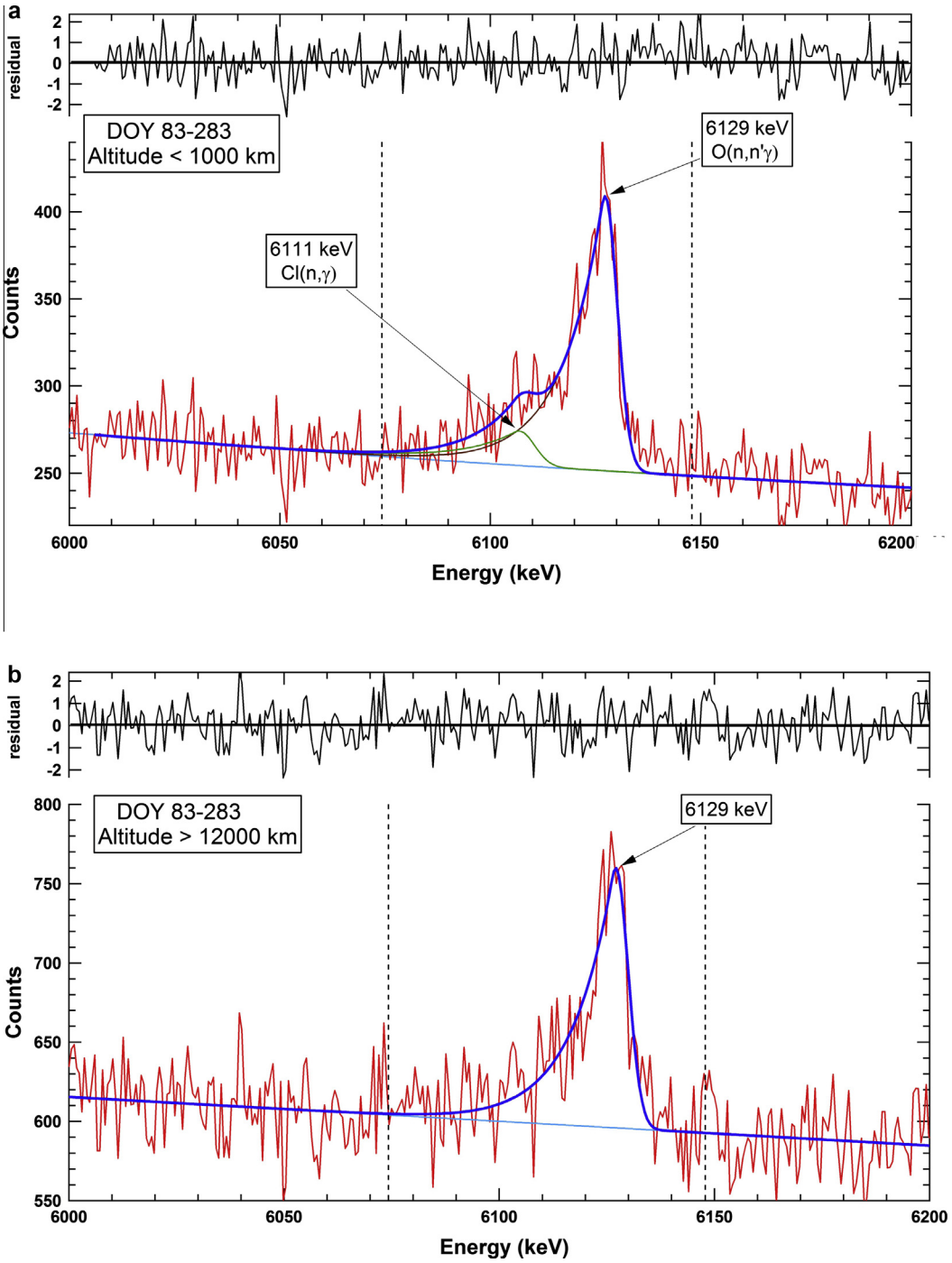

Fig. 3. Fit to peaks in the energy range of the 6111-keV Cl peak. (a) Low-altitude spectrum; and (b) high-altitude spectrum. The large peak at 6129 keV is due to an inelastic scatter reaction in oxygen. Other conventions follow those in Fig. 2.

(Boynton et al., 2007). There is no comparable ground-truth value for Mercury, but Si is a major element that generally varies less than other major elements (Peplowski et al., 2012a). For this reason, elemental abundances determined for Mercury are normalized to Si. In this analysis, the abundance of chlorine was determined with the forward calculation. Then, the element abundance was normalized to the Si abundance determined from the Si neutron capture gamma ray. This determination was made under the assumptions that all neutron capture cross sections have identical energy dependence and that any uncertainty in the macroscopic cross-section used in the forward model calculation is corrected by this method. Fortunately, the model composition has a macroscopic cross section consistent with that inferred from thermal neutron measurements (Lawrence et al., 2010; Peplowski et al., 2015) despite a Cl concentration lower than measured.

5. Results

The GRS spectrum used to determine the bulk Cl abundance includes data from more than three full Mercury sidereal days (~177 Earth days) and represents a largely uniform coverage of the surface as a function of longitude, but coverage in latitude is variable because of MESSENGER's highly eccentric orbit. The

Table 1
Results of fits to the chlorine peaks for a summed spectrum for the time period 24 March–10 October 2011.

	Element	Energy (keV)	Count rate[a]	Uncertainty[a]
Northern hemisphere	Cl	1955	0.067	0.020
	Cl	6111[b]	0.093	0.026
	Si	3539	0.164	0.016
0–60°N	Cl	1955	0.052	0.024
	Cl	6111[b]	0.088	0.027
	Si	3539	0.159	0.017
80–90°N	Cl	1955	0.110	0.065
	Cl	6111[b]	0.192	0.068
	Si	3539	0.122	0.039

[a] Count rate and uncertainty in counts/min.
[b] Count rates are for the sum of the photopeak and escape peaks and corrected for interferences.

Table 2
Chlorine abundances for selected regions on Mercury.

Spatial coverage	Cl/Si	Cl wt%[a]
Northern hemisphere	0.0057 ± 0.0010	0.14 ± 0.03
0–60°N	0.0049 ± 0.0010	0.12 ± 0.03
80–90°N	0.014 ± 0.005	0.35 ± 0.13

[a] Cl wt% – for a Si abundance of 24.6 wt%.

periapsis of the orbit was generally between 60°N and 70°N and the periapsis altitude varied from ~200 km to ~500 km. The derived Cl results can be regarded as representing the mean value for sampled regions north of Mercury's equator.

We used the techniques described above and given by Evans et al. (2012) to determine the mean abundance of Cl in the northern hemisphere (Table 2). The derived mean abundance, by mass, is Cl/Si = 0.0057 ± 0.001, where the uncertainty is one standard deviation and reflects a combination of statistical uncertainty derived from the peak areas and the background continuum together with the goodness of fit to the measurements (Evans et al., 2012). As with most of the other elements determined from GRS measurements (except for K), the count rates in the Cl peaks were not sufficient to map the Cl abundance, even at a reduced spatial resolution. However, as for the GRS Na analysis (Peplowski et al., 2014), we were able to derive Cl abundances for varying latitude ranges and found evidence for an enhancement in the north-polar region relative to equatorial latitudes. Cl/Si abundance ratios for latitude bins of 0–60°N and 80–90°N, shown in Table 2, highlight this observation. The Cl/Si ratio for the polar region is higher than that at mid-latitudes by a factor of 2.9 ± 1.3. A similar increase with latitude in the Na/Si ratio (by a factor of 1.85 ± 0.32) has previously been reported (Peplowski et al., 2014), which when combined with the K abundance map of Peplowski et al. (2011) highlight a trend of elevated abundances of moderately volatile element at high northern latitudes. This similar latitude dependence could be interpreted as indicating that the Cl distribution has the same cause as the Na and/or K distributions, either an association with the large expanse of northern volcanic plains (Head et al., 2011) or a result of the thermal redistribution of volatile elements on the surface of Mercury (Peplowski et al., 2011). The latter may be less likely for Na (Weider et al., 2015), though this inference does not rule out a thermal redistribution scenario for Cl.

6. Discussion

6.1. Chlorine as a test of Mercury's accretion history

Many hypotheses for the formation of Mercury put forward prior to the MESSENGER mission invoked high-temperature processes to account for the planet's large ratio of metal to silicate (e.g., Taylor and Scott, 2003), and some of these hypotheses predict that the planet should be depleted in volatile elements. On the basis of Mercury's K/Th ratio, Peplowski et al. (2011) ruled out formation mechanisms for Mercury that involved extreme and prolonged heating of the planet or its precursor materials. However, there is a possibility that a giant impact could have yielded Mercury's high metal-to-silicate ratio without severe volatile depletion of the target planet (Stewart et al., 2013).

The overwhelming evidence from the MESSENGER GRS and XRS measurements is that the volatile elements, S, K, Na, and Cl are not depleted on the surface of Mercury relative to other terrestrial planetary bodies. Moreover, the volatile element chemistry of Mercury's surface materials provides important constraints for models of its formation. The Cl/K ratio is a particularly useful tool for testing formation models, for three reasons: (1) abundances of Cl and K are expected to be related during igneous processes, as both are incompatible, moderately volatile lithophile elements (Lodders, 2003); (2) Cl has a higher susceptibility to escape from planetary surfaces during accretion processes than other volatile elements such as K, Na, and S (Sharp and Draper, 2013); and (3) there is evidence that Cl is more susceptible to loss by thermal processing, for example, ordinary chondrites and enstatite chondrites display generally lower Cl/K ratios than the more volatile-rich carbonaceous chondrites (Fig. 4). Consequently, the Cl/K ratios 1.22 (0–60°N) and 1.96 (>80°N) for Mercury may provide constraints on the nature and timing of Mercury's accretion history.

Mars, long regarded as among the most volatile-rich of the planets in the inner Solar System, has a Cl/K ratio approximately equal to that of CI chondrites (Fig. 4). Furthermore, on the basis of Hf–W isotope systematics Mars is thought to have formed within a few million years and to have reached nearly its final size

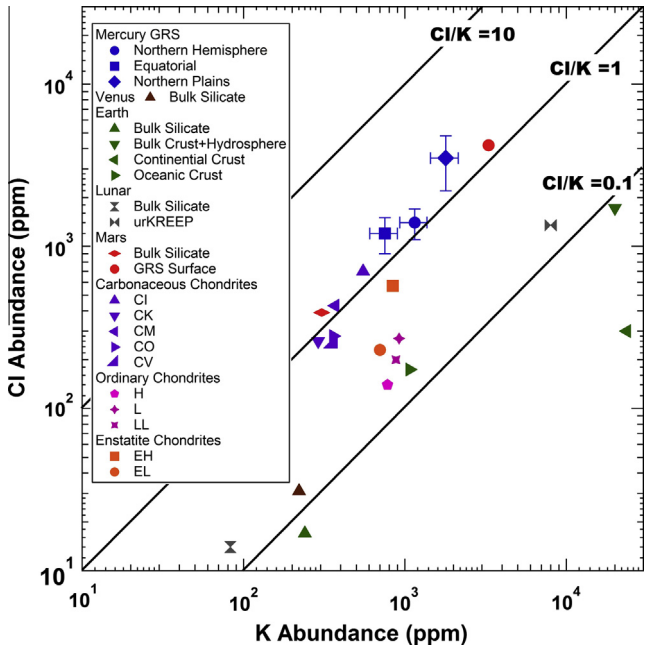

Fig. 4. Relationship between Cl and K for Mercury (dark blue symbols) and other Solar System objects. Values are shown for Venus in brown, Earth in green, Mars in red, carbonaceous chondrites in purple, ordinary chondrites in pink, and enstatite chondrites in orange. Data for this figure for Venus are from Morgan and Anders (1980); Earth, McDonough and Sun (1995) and Lodders and Fegley (1998); the Moon, Taylor (1982), Warren (1988), and McCubbin et al. (in press); Mars, Boynton et al. (2007) and Taylor et al. (2010); chondrites Lodders and Fegley (1998); and Mercury, Peplowski et al. (2011). Lines of constant Cl/K are shown for reference.

before the dissipation of nebular gas; it should therefore, not have experienced depletion in highly volatile elements from collisional removal during accretion (Dauphas and Pourmand, 2011). In contrast, Earth and the Moon, which have subchondritic Cl/K ratios (Fig. 4), had protracted impact and accretion histories consistent with stripping of Cl from their surfaces (Sharp and Draper, 2013). Stripping of Cl from the Moon during accretion is further supported by isotopic enrichments in ^{37}Cl relative to ^{35}Cl in KREEP-rich lunar rocks and impact breccias (Sharp et al., 2010; McCubbin et al., in press).

Mercury has a chondritic Cl/K ratio, similar to that of Mars (Fig. 4), indicating that it, too, has been spared the loss of volatile elements through collisional erosion, a result that may suggest a similarly limited history of major impacts. A more limited impact history for Mercury is also supported by a deficit in large impact basins compared with the Moon (Fassett et al., 2012). The timing of any impact event invoked for an early stripping of Mercury's mantle would thus be constrained to have occurred before dissipation of nebular gas. However, such an impact must occur after differentiation of Mercury's core, requiring exceptionally rapid accretion and core formation, on the order of a few million years. Differentiation on these rapid timescales would have been facilitated by the decay of ^{26}Al. Of course, a giant impact event need not have been responsible for the elevated metal-to-silicate ratio on Mercury. The surface abundances of S and Fe determined from MESSENGER data suggest that Mercury formed from chemically reduced metal-rich precursor material (Nittler et al., 2011). Such material must have had Cl/K values consistent with the observed concentrations on Mercury's present surface, as K and Cl are lithophile and incompatible and would have fractionated into magmas that contributed to the crust in the same ratio as that originally accreted.

6.2. Chlorine as a magmatic volatile

Magmatic volatiles, including H, C, N, F, S, and Cl, play important roles in the production, transport, and eruption of molten materials in terrestrial planetary bodies. Mercury exhibits geomorphic evidence that volatile-assisted explosive volcanic eruptions have occurred in the past (Kerber et al., 2009; Goudge et al., 2014; Thomas et al., 2014). Furthermore, the high abundance of S on Mercury's surface, compared with igneous rocks on other terrestrial planets (Nittler et al., 2011; Evans et al., 2012; Weider et al., 2012), has been attributed to a low oxygen fugacity in Mercury's mantle and an enhanced solubility of S in silicate liquids at low fO_2 (McCubbin et al., 2012; Zolotov et al., 2013). Chlorine is another important magmatic volatile on Earth and Mars (Carroll and Webster, 1994; Webster et al., 1999; Aiuppa et al., 2009; Filiberto and Treiman, 2009; McCubbin et al., 2013), and it has been proposed to be an important magmatic volatile on Mercury (Zolotov, 2011). The high Cl concentrations on Mercury's surface present an opportunity to explore this hypothesis.

Our observations indicate that the abundance of Cl in the regions north of 80°N is about three times that in the region between 0° and 60°N (Table 2). One of the most prominent geologic units in the northern region of Mercury is the northern volcanic plains (NVP), one of the largest expanses of smooth plains on the planet (Denevi et al., 2013). This unit is less cratered than its surroundings and is not obviously associated with an impact basin. On the basis of a variety of morphological evidence, the NVP unit is thought to be the product of one or more episodes of flood volcanism (Head et al., 2011). On Earth, flood volcanism is generally produced by partial melting of mantle material and high rates of eruption of mantle-derived magma onto the surface. MESSENGER XRS and GRS measurements of Mg/Si, Al/Si, and Ca/Si ratios indicate that the NVP have surface compositions intermediate between low-Fe basalts and komatiities on Earth (Nittler et al., 2011; Stockstill-Cahill et al., 2012). Maps derived from XRS and GRS measurements have revealed a geochemical terrane at high northern latitudes (Weider et al., 2015; Peplowski et al., 2015) that hosts elevated concentrations of thermal neutron absorbers consistent with our observation of an elevated abundance of Cl. As this terrane is dominated by the NVP, and because magmatic volatiles commonly aid in the eruption of magmas, it is logical to hypothesize that Cl may be an important contributor. However, the spatial extent of the northern flood plains is not a precise match to the northern geochemical terrane, complicating any attempt to link geochemistry, including Cl abundance, with the formation of the plains unit (Peplowski et al., 2015; Weider et al., 2015). The observed Cl enrichment at high northern latitudes, and presumably in NVP material, could reflect chlorine's incompatible behavior in magmatic systems, i.e., its preferential accumulation in melts during formation and crystallization of magmas. Other magmatic volatiles such as H, F, and N could also have played a role, but to date they have not been detected by MESSENGER, except for the detection of H in polar deposits within permanently shadowed portions of the interiors of impact craters in the north polar region (Lawrence et al., 2013).

The elevated Cl abundance at high latitudes could reflect an accumulation of volcanic gas condensates in near-surface materials. The detection of abundant Cl compounds emitted from enstatite chondrite melts (Muenow et al., 1992) is consistent with this notion. On Earth and Mars, Cl mainly degases as HCl (Aiuppa et al., 2009) whereas in H-depleted melts Cl mainly degases as S–Cl and metal chloride compounds. Thermodynamic modeling by Fegley and Zolotov (2000) showed that NaCl, KCl, $(NaCl)_2$ and $(KCl)_2$ could be the major Cl-bearing volcanic gases on Io. This finding is consistent with the detection of Na, K, and Cl in Io's atmosphere and torus (Küppers and Schneider, 2000; Lellouch et al., 2003), and with NaCl grains in the jovian system (Postberg et al., 2006). Depending on vent pressure, NaCl and KCl condense at temperatures below ~1000−1500 K (Fegley and Zolotov, 2000). These temperatures are similar to those at the top of a cooling flow of basaltic or komatiitic lava. Speciation models for metal-free volcanic gases (Zolotov, 2011) show that Mercury's lavas could emit Cl_2, Cl, SCl_2, and S_2Cl. Including Na and K in the modeled system shows that NaCl, $(NaCl)_2$ and KCl could be the major Cl-bearing gases, especially at elevated temperatures and high abundances of alkali elements (Fig. 5).

These results indicate that condensation of NaCl at magmatic temperatures is common and that condensation of NaCl and KCl from cooling gases can occur at much lower temperature at low-pressure, near-surface conditions (cf. Fegley and Zolotov, 2000). In addition to NaCl and KCl, chlorides of Mg and, especially Fe^{2+}, are highly volatile (Fig. 6), in agreement with recent experiments (DiFrancesco et al., 2015). These species could be among Mercury's magmatic gases, reflecting Cl-metal melt complexes with a salt-like ionic bonding (Carroll and Webster, 1994; Evans et al., 2008). The degassing of metal chlorides from thick lava flows in Mercury's NVP region and subsequent condensation could enrich the upper meter of volcanic material in Cl, Na, K, Mg, and Fe. This interpretation is consistent with the high measured concentrations of Cl, Na (Peplowski et al., 2014), and K (Peplowski et al., 2012a) in the northern hemisphere and in parts of the NVP.

6.3. Chlorine geochemical behavior at Mercury's oxygen fugacity conditions

The oxygen fugacity conditions of Earth, the Moon, and Mars range from one $\log_{10}$ unit below the iron–wüstite (IW) buffer to several $\log_{10}$ units above the quartz–fayalite–magnetite (QFM) buffer (Wadhwa, 2008; Sharp et al., 2013). Mercury, however,

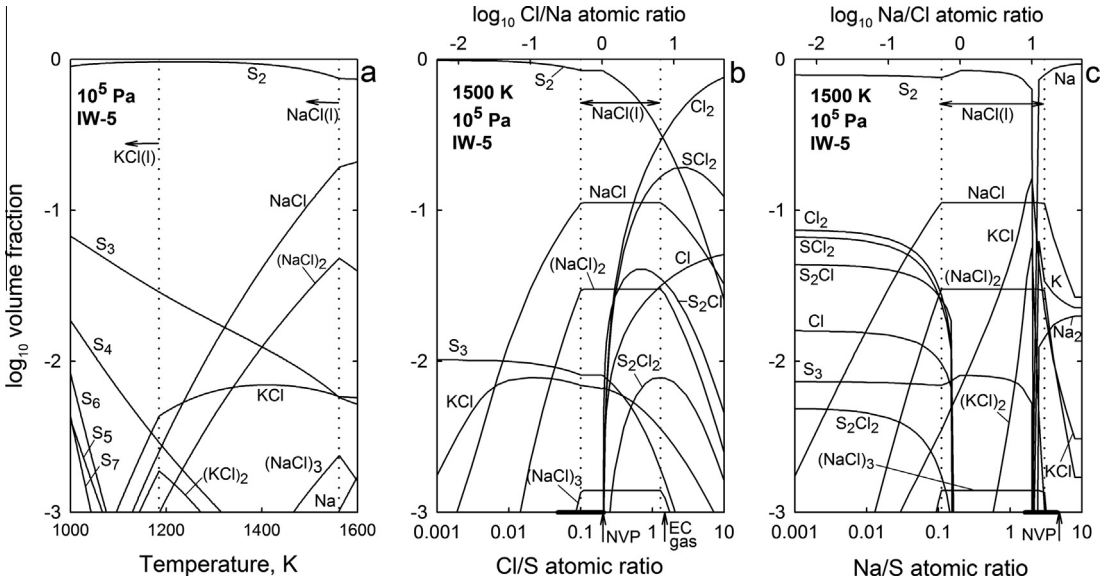

Fig. 5. Speciation of Cl in the S–O–Cl–Na–K system, taken as a model for potential volcanic gases on Mercury at 1 bar total pressure and an O_2 fugacity of 5 $\log_{10}$ units below the iron-wüstite (IW) buffer. (a) The effect of temperature on the speciation of the system S:Cl:Na:K = 1:0.2:0.2:0.004. (b) The effect of Cl/S ratio at S:Na:K = 1:0.2:0.004 and 1500 K. (c) The effect of Na/S ratio at S:Cl:K = 1:0.2:0.004 and 1500 K. Vertical dotted lines indicate conditions of condensation of liquid NaCl and KCl. In (b) and (c), the bold lines along portions of the bottom of the panel show atomic ratios measured in Mercury's surface materials (Weider et al., 2012; Peplowski et al., 2014; this work). Vertical arrows show elemental ratios in the NVP and degassing products of enstatite chondrite (EC) melts (Muenow et al., 1992). The assumed composition of the nominal system incorporates Cl/S and Na/K ratios equal to those in the NVP (Weider et al., 2012; Peplowski et al., 2012a, 2014; this work) and an Na/S ratio equal to that in enstatite and carbonaceous chondrites. The speciation calculations were performed with codes and data described by Fegley and Zolotov (2000) and Zolotov (2011).

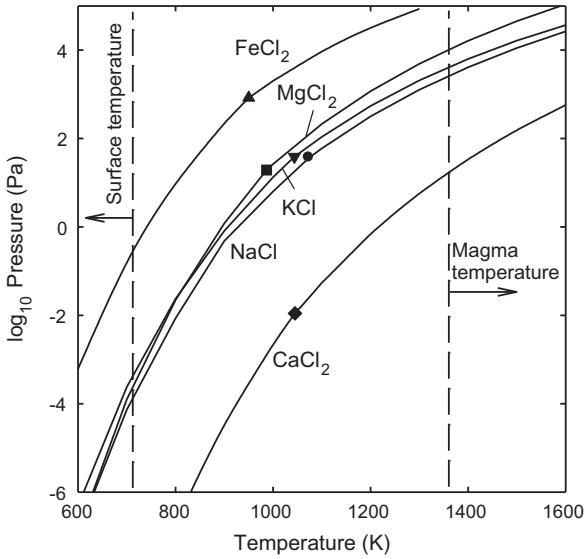

Fig. 6. Partial pressures of metal chloride gases calculated to be in equilibrium with condensed chlorides. Thermodynamic data are from Barin (2004). The symbols correspond to melting temperatures of chlorides.

appears to be much more reduced and is thought to be outside this range; its fO_2 is estimated to be in the range from 3 to 7 $\log_{10}$ units below the IW buffer (McCubbin et al., 2012; Zolotov et al., 2013). Chlorine is typically insensitive to redox changes in most high-temperature igneous and hydrothermal systems because it remains stable as a monovalent anion under a wide range of geologic processes. Its behavior in geologic systems can change markedly as a function of oxygen fugacity, however, given its geochemical affinity for redox-sensitive elements (e.g., H, Fe, P, and S). The implications of each of these geochemical affinities and the roles they may have played on Mercury warrant discussion.

Chlorine is highly hydrophilic, and chloride salts exhibit very high solubility in aqueous and hydrothermal solutions. Under highly reducing conditions, such as those inferred for Mercury, H_2O is unstable, and the dominant H-species is H_2. Little is known regarding the behavior of Cl in H_2 dominated fluids or vapors, so it is unclear whether Cl would retain its hydrophilic nature under conditions relevant to Mercury. Additionally, the aqueous redistribution of Cl that has been observed on Earth and Mars (Taylor et al., 2010; Sharp and Draper, 2013) is not likely to have occurred on Mercury. On Mercury, chlorine is more likely redistributed during volcanic processes, perhaps in a manner similar to that on the Moon, where H_2 was also the dominant H species (rather than H_2O) during degassing (Elkins-Tanton and Grove, 2011; Sharp et al., 2013; Shearer et al., 2014).

Chlorine abundances are often positively correlated with Fe abundances in silicate minerals, such as amphiboles and micaceous minerals (Morrison, 1991; Mazdab, 2003). This affinity is the result of the larger ionic radius of Fe^{2+} (compared with Mg^{2+}), which allows the crystal structures of these minerals to accommodate the large ionic radius of Cl^- (Cl^- typically substitutes for OH^- or F^- in most silicate minerals). This crystal chemical rule, known as the Mg-avoidance principle (Morrison, 1991), may have important implications for the mineralogy of Cl on Mercury. The low fO_2 of Mercury means that most Fe exists as Fe metal or sulfide, and that the abundance of FeO components in ferromagnesian silicates is very low. That the 1-μm absorption feature in reflectance spectra diagnostic of FeO crystal-field absorptions in ferromagnesian silicates is not seen on Mercury (e.g., Robinson et al., 2008; Riner et al., 2010; Izenberg et al., 2014) further supports the reduced nature of Fe on the planet. Ferromagnesian silicates are unlikely to be a possible mineralogical host for Cl on Mercury.

Chlorine might alternately be bound in lawrencite ($FeCl_2$), which has been observed as a sublimate on Mt. Vesuvius, as akaganeite from iron meteorites, within hydrothermally altered lunar regolith, and in native iron from Greenland (Gaines et al., 1997; Shearer et al., 2014). The high volatility of $FeCl_2$ (Fig. 6) suggests that the presence of lawrencite among volcanic gas condensates

in surface and near-surface volcanic materials is possible. In addition, lawrencite is the most probable chloride mineral that could be sublimated into the exosphere in Sun-warmed regions.

One of the most ubiquitous mineralogical hosts for Cl in the Solar System is the phosphate mineral apatite, $Ca_5(PO_4)_3(F, Cl, OH)$. Under highly reducing conditions, however, P loses its lithophile characteristic and becomes more siderophilic (Pasek, 2015). Consequently, P is primarily hosted in metallic phases in highly reduced systems, either as a dissolved component in metal or exsolved as crystals of the phosphide schreibersite, $(Fe, Ni)_3P$. In fact, most of the chlorapatite in ordinary chondrites is secondary. It forms through hydrothermal alteration that involves oxidation of primary P-bearing metal to the volatile-free phosphate mineral merrillite $[Ca_{18}Na_2Mg_2(PO_4)_{14}]$, followed by alteration of the merrillite by Cl-rich fluids to form apatite (Jones et al., 2014). Given the low oxygen fugacity of Mercury's surface material, apatite is unlikely to be a primary magmatic mineralogical sink for Cl, although it may occur in portions of the regolith that have experienced locally elevated fO_2 and alteration by Cl-rich fluids.

As discussed above, alkali halides, such as halite (NaCl) and sylvite (KCl), may also represent mineralogical hosts for Cl in Mercury's crystallized igneous rocks (Zolotov, 2011). Although these minerals are normally associated with aqueous processes on Earth and Mars, halides might form at the exceptionally low oxygen fugacities of Mercury. The observation that the northern regions of Mercury, which display an enriched Cl abundance, are also enriched in alkali elements K and Na (Peplowski et al., 2012a, 2014; Evans et al., 2012) might imply the presence of alkali chlorides. However, it is also possible that these halide compounds present in the magma were subsequently incorporated into other crystallizing phases. The potential stability of chlorides over geologic time on Mercury is unknown. At the maximum surface temperature (700 K), partial pressures of NaCl and KCl above corresponding solids are only $10^{-3.1}$ and $10^{-7.6}$ Pa, respectively (Fig. 6), and a significant sublimation-driven transport may not occur. However, some of the Na, K, and Cl could be sputtered from surface chlorides by the impact of high-energy ions and micrometeoroids.

Chlorine is not typically considered a chalcophile element, but in some highly reduced enstatite chondrites and achondrites, which have been suggested as possible meteoritical analogs for Mercury's silicate fraction and/or its precursory materials (Taylor and Scott, 2003), Cl is present in the sulfide phase djerfisherite, $(K, Na)_6(Na, Li, Cu, Fe, Ni)(Fe, Cu, Ni)_{24}S_{26}Cl$ (Fuchs, 1966; Ebel and Sack, 2013). Djerfisherite also hosts alkali elements (Na, K, and Li), which supports geochemical links between K and Cl even in highly reduced systems. It is possible that the halides were incorporated with djerfisherite during crystallization from a melt. Consequently, sulfides may be a mineralogical host for Cl on Mercury, especially given the elevated abundances of S on much of Mercury's surface (Nittler et al., 2011). However, limited mapping of the abundance of S in the NVP shows low values (Weider et al., 2015). This approximate anti-correlation between S and Cl abundances at high northern latitudes on Mercury suggests that Cl-bearing sulfides, if present, are not the dominant sulfide phase, consistent with the inference that Ca and/or Mg sulfides dominate the sulfide component on the surface of Mercury (Nittler et al., 2011; Weider et al., 2012, 2015).

6.4. Chlorine and thermal neutron measurements

Although not directly related to Mercury's formation and evolution, there is an interesting interpretation of the chlorine abundances. Measurements of thermal neutrons acquired by MESSENGER's Neutron Spectrometer (NS) during the spacecraft's flybys of Mercury indicated higher-than-expected abundances of neutron absorbers on Mercury's surface (Lawrence et al., 2010). Those authors suggested that the source may be elevated metal content, perhaps in the form of an oxide, e.g.; ilmenite ($FeTiO_3$) at the 7–18 wt% level. However, subsequent orbital measurements by both the GRS and XRS (Nittler et al., 2011; Evans et al., 2012; Weider et al., 2014) have shown that the abundances of Fe and Ti are too low to be consistent with such abundances of ilmenite. The presence of ilmenite is also inconsistent with the low oxidation state of Mercury's surface (Riner et al., 2010; McCubbin et al., 2012; Zolotov et al., 2013), leaving the identity of the neutron absorbing elements uncertain. Chlorine, with a large thermal neutron capture cross-section (~200 times that of Si, and ~10 times that of Fe), provides a ready explanation for the high thermal neutron absorption of Mercury's surface indicated by the NS flyby results. Furthermore, recent measurements of thermal neutron variability across Mercury's northern hemisphere (Peplowski et al., 2015) show an enhancement at Mercury's north polar region that is consistent with our reported Cl enhancement there. By understanding the relationship between thermal neutron measurements and Cl measurements, we are able to extend our knowledge of the spatial distribution of Cl beyond the GRS results (Peplowski et al., 2015).

7. Conclusions

The abundance of chlorine on the surface of Mercury has been determined for the first time from an analysis of MESSENGER GRS measurements. The Cl abundance is some three times greater at high northern latitudes than in mid- and equatorial latitude bands. Thermal neutron absorption also shows an enhancement in Mercury's north polar region, a result consistent with the elevated Cl abundances. On the basis of the known surface composition of Mercury, chlorine appears to be a major contributor to the total neutron absorption of Mercury's surface material. This situation contrasts with that on the Moon where iron, titanium, and rare-earth elements (Gd, Sm) dominate thermal neutron absorption.

Our results provide further evidence that volatile elements (e.g., S, K, Na, and Cl) are not depleted on the surface of Mercury, and instead are present at abundances similar to those on other terrestrial planetary bodies. Mercury has a chondritic Cl/K ratio, indicating that it has not experienced loss of volatile elements through collisional erosion. Given that Cl is particularly susceptible to loss through collisional erosion compared with other volatile elements (K, S, Na) (Sharp and Draper, 2013) we infer that Mercury had a limited impact history and underwent rapid accretion and differentiation, likely powered by the radioactive decay of ^{26}Al. We have also evaluated potential mineralogical hosts of Cl on Mercury and can rule out primary apatite, mica, and amphiboles, as well as aqueously deposited halides as possible mineralogical hosts for Cl. Among the remaining candidate hosts are alkali halides, such as halite or sylvite, formed through igneous processes of volcanic degassing and condensation, the iron halide lawrencite, and the sulfide djerfisherite. To evaluate these possibilities further would likely require in situ analysis by landers or rovers on Mercury, a Mercury sample return mission, or the discovery of one or more meteorites from Mercury.

Acknowledgments

This work was supported by the NASA Discovery Program under contracts NAS5-97271 to The Johns Hopkins University Applied Physics Laboratory and NASW-0002 to the Carnegie Institution of Washington. All of the data used in the present study are available in the Planetary Data System (PDS). Support was also provided to

LGE, DJL, LRN, and RDS by the MESSENGER Participating Scientist Program. FMM and DSE acknowledge support from the NASA Cosmochemistry Program during this study (through grants NNX14AK43G and NNX10AI42G, respectively). We especially thank the dedicated MESSENGER operations team for their continued support of this mission.

References

Aiuppa, A., Baker, D.R., Webster, J.D., 2009. Halogens in volcanic systems. Chem. Geol. 263, 1–18.

Barin, I., 2004. Thermochemical Data of Pure Substances. Wiley, New York, 2400 pp.

Boynton, W.V. et al., 2007. Concentration of H, Si, Cl, K, Fe, and Th in the low- and mid-latitude regions of Mars. J. Geophys. Res. 112, E12S99. http://dx.doi.org/10.1029/2007JE002887.

Brückner, J. et al., 1991. Proton-induced radiation damage in germanium detectors. IEEE Trans. Nucl. Sci. 38, 209–217.

Carroll, M.R., Webster, J.D., 1994. Solubilities of sulfur, noble gases, nitrogen, chlorine, and fluorine in magmas. In: Carroll, M.R., Holloway, J.R. (Eds.), Volatiles in Magmas. Rev. Mineral. 30, Mineral Soc. Am., Washington, DC, pp. 231–280.

Dauphas, N., Pourmand, A., 2011. Hf–W–Th evidence for rapid growth of Mars and its status as a planetary embryo. Nature 473, 490–492. http://dx.doi.org/10.1038/nature10077.

Denevi, B.W. et al., 2013. The distribution and origin of smooth plains on Mercury. J. Geophys. Res. Planets 118, 891–907. http://dx.doi.org/10.1029/2012JE004295.

DiFrancesco, N.J. et al., 2015. Simulating a martian fumarole: Understanding the effects of a degassing martian magma on surrounding rock. Lunar Planet. Sci. 46, 2305.

Ebel, D.S., Sack, R.O., 2013. Djerfisherite: Nebular source of refractory potassium. Contrib. Mineral Petrol. 166, 923–934. http://dx.doi.org/10.1007/s00410-013-0898-x.

Elkins-Tanton, L.T., Grove, T.L., 2011. Water (hydrogen) in the lunar mantle: Results from petrology and magma ocean modeling. Earth Planet. Sci. Lett. 307, 173–179.

Evans, L.G., Reedy, R.C., Trombka, J.I., 1993. Introduction to planetary remote sensing gamma ray spectroscopy. In: Pieters, C.M., Englert, P.A.J. (Eds.), Remote Geochemical Analysis: Elemental and Mineralogical Composition. Cambridge Univ. Press, New York, pp. 167–198.

Evans, K.A. et al., 2008. A preliminary investigation of chlorine XANES in silicate glasses. Geochem. Geophys. Geosyst. 9, Q10003. http://dx.doi.org/10.1029/2008GC002157.

Evans, L.G. et al., 2006. Analysis of gamma ray spectra measured by Mars Odyssey. J. Geophys. Res. 111, E03S04. http://dx.doi.org/10.1029/2005JE002657.

Evans, L.G. et al., 2012. Major-element abundances on the surface of Mercury: Results from the MESSENGER Gamma-Ray Spectrometer. J. Geophys. Res. Planets 117, E00L07. http://dx.doi.org/10.1029/2012JE004178.

Fassett, C.J. et al., 2012. Large impact basins on Mercury: Global distribution, characteristics, and modification history from MESSENGER orbital data. J. Geophys. Res. 117, E00L08. http://dx.doi.org/10.1029/2012JE004154.

Fegley Jr., B., Zolotov, M.Yu., 2000. Chemistry of sodium, potassium, and chlorine as volcanic gases on Io. Icarus 148, 193–210.

Filiberto, J., Treiman, A.H., 2009. Martian magmas: Water-poor but chlorine-rich. Geology 37, 1087–1090.

Fuchs, L.H., 1966. Djerfisherite, alkali-copper sulfide: A new mineral from enstatite chondrites. Science 153, 166–167.

Gaines, R.V. et al., 1997. Dana's New Mineralogy, eighth ed. John Wiley and Sons, New York, NY, 1872 pp.

Goldsten, J.O. et al., 2007. The MESSENGER Gamma-ray and Neutron Spectrometer. Space Sci. Rev. 131, 339–391. http://dx.doi.org/10.1007/s11214-007-9262-7.

Goudge, T.A. et al., 2014. Global inventory and characterization of pyroclastic activity from MESSENGER orbital data. J. Geophys. Res. Planets 119, 635–658. http://dx.doi.org/10.1002/2013JE004480.

Head, J.W. et al., 2008. Volcanism on Mercury: Evidence from the first MESSENGER flyby. Science 321, 69–72. http://dx.doi.org/10.1126/science.1159256.

Head, J.W. et al., 2011. Flood volcanism in the northern high latitudes of Mercury revealed by MESSENGER. Science 333, 1853–1856. http://dx.doi.org/10.1126/science.1211997.

Izenberg, N.R. et al., 2014. The low-iron reduced surface of Mercury as seen in spectral reflectance by MESSNGER. Icarus 228, 364–374. http://dx.doi.org/10.1016/j.icarus.2013104.023.

Jones, R.H. et al., 2014. Phosphate minerals in LL chondrites: A record of the action of fluids during metamorphism on ordinary chondrite parent bodies. Geochim. Cosmochim. Acta 132, 120–140.

Keller, J.M. et al., 2006. Equatorial and mid-latitude distribution of chlorine measured by Mars Odyssey GRS. J. Geophys. Res. 111, E03S08. http://dx.doi.org/10.1029/2005JE002679.

Kerber, L. et al., 2009. The global distribution of pyroclastic deposits on Mercury; the view from MESSENGER flybys 1–3. Planet. Space Sci. 59, 1895–1909. http://dx.doi.org/10.1016/j.pss.2011.03.020.

Küppers, M., Schneider, N.M., 2000. Discovery of chlorine in the Io torus. Geophys. Res. Lett. 27, 513–516.

Lawrence, D.J. et al., 2010. Identification and measurement of neutron-absorbing elements on Mercury's surface. Icarus 209, 195–200. http://dx.doi.org/10.1016/j.icarus.2010.04.055.

Lawrence, D.J. et al., 2013. Evidence for water ice near Mercury's north pole from MESSENGER Neutron Spectrometer measurements. Science 339, 292–296. http://dx.doi.org/10.1126/science.1229953.

Lellouch, E. et al., 2003. Volcanically emitted sodium chloride as a source for Io's neutral clouds and plasma torus. Nature 421, 45–47.

Lodders, K., 2003. Solar System abundances and condensation temperatures of the elements. Astrophys. J. 591, 1220–1247.

Lodders, K., Fegley Jr., B., 1998. The Planetary Scientist's Companion. Oxford University Press, New York, 400 pp.

Mazdab, F.K., 2003. The diversity and occurrence of potassium-dominant amphiboles. Can. Mineral. 41, 1329–1344.

McCubbin, F.M., Riner, M.A., Vander Kaaden, K.E., 2012. Is Mercury a volatile-rich planet? Geophys. Res. Lett. 39, L090202. http://dx.doi.org/10.1029/2012GRL051711.

McCubbin, F.M. et al., 2013. A petrogenetic model for the co-magmatic origin of chassignites and nakhlites: Inferences from chlorine-rich minerals, petrology, and geochemistry. Meteorit. Planet. Sci. 48, 819–853.

McCubbin, F.M., et al., 2015. Magmatic volatiles (H, C, N, F, S, Cl) in the lunar mantle, crust, and regolith: Abundances, distributions, processes, and reservoirs, Amer. Mineral. (in press). http://dx.doi.org/10.2138/am-215-4934.

McDonough, W.F., Sun, S.S., 1995. The composition of the Earth. Chem. Geology 120, 223–253.

McKinney, G.W. et al., 2006. MCNPX benchmark for cosmic ray interactions with the Moon. J. Geophys. Res. 111, E06004. http://dx.doi.org/10.1029/2005JE002551.

Morgan, J.W., Anders, E., 1980. Chemical composition of Earth, Venus, and Mercury. Proc. National Acad. Sci. 77, 6973–6977.

Morrison, J., 1991. Compositional constraints on the incorporation of Cl into amphiboles. Amer. Mineral. 76, 1920–1930.

Muenow, D.W., Keil, K., Wilson, L., 1992. High-temperature mass spectrometric degassing of enstatite chondrites: Implications for pyroclastic volcanism on the aubrite parent body. Geochim. Cosmochim. Acta 56, 4267–4280.

Nittler, L.R. et al., 2011. The major element composition of Mercury's surface from MESSENGER X-ray spectrometry. Science 333, 1847–1850. http://dx.doi.org/10.1126/science.1211567.

Pasek, M.A., 2015. Phosphorus as a lunar volatile. Icarus 255, 18–23. http://dx.doi.org/10.1016/j.icarus.2014.07.031.

Peplowski, P.N. et al., 2011. Radioactive elements on Mercury's surface from MESSENGER: Implications for the planet's formation and evolution. Science 333, 1850–1852. http://dx.doi.org/10.1126/science.1211576.

Peplowski, P.N. et al., 2012a. Variations in the abundances of potassium and thorium on the surface of Mercury: Results from the MESSENGER Gamma-Ray Spectrometer. J. Geophys. Res. 117, E00L04. http://dx.doi.org/10.1029/2012JE004141.

Peplowski, P.N. et al., 2012b. Aluminum abundance on the surface of Mercury: Application of a new background-reduction technique for the analysis of gamma-ray spectroscopy data. J. Geophys. Res. 117, E00L10. http://dx.doi.org/10.1029/2012JE004181.

Peplowski, P.N. et al., 2014. Enhanced sodium in Mercury's north polar region revealed by the MESSENGER Gamma-Ray Spectrometer. Icarus 228, 86–95. http://dx.doi.org/10.1016/j.icarus.2013.09.007.

Peplowski, P.N. et al., 2015. Geochemical terranes of Mercury's northern hemisphere as revealed by MESSENGER neutron measurements. Icarus 253, 346–363. http://dx.doi.org/10.1016/j.icarus.2015.02.002.

Postberg, F. et al., 2006. Composition of jovian dust stream particles. Icarus 183, 122–134.

Riner, M.A. et al., 2010. Mercury surface composition: Integrating petrologic modeling and remote sensing data to place constraints on FeO abundance. Icarus 209, 301–313.

Robinson, M.S. et al., 2008. Reflectance and color variation on Mercury: Regolith processes and compositional heterogeneity. Science 321, 66–69.

Sharp, Z.D., Draper, D.S., 2013. The chlorine abundance on Earth: Implications for a habitable planet. Earth Planet. Sci. Lett. 369–370, 72–77. http://dx.doi.org/10.1016/j.epsl.2013.03.005.

Sharp, Z.D. et al., 2010. An experimental determination of chlorine isotope fractionation in acid systems and applications to volcanic fumaroles. Geochim. Cosmochim. Acta 74, 264–273.

Sharp, Z.D. et al., 2013. A hydrogen-based oxidation mechanism relevant to planetary formation. Earth Planet. Sci. Lett. 380, 88–97. http://dx.doi.org/10.1016/j.epsl.2013.08.015.

Shearer, C.K. et al., 2014. Chlorine distribution and its isotopic composition in "rusty rock" 66095: Implications for volatile element enrichment of "rusty rock" and lunar soils, origin of "rusty" alteration, and volatile element behavior on the Moon. Geochim. Cosmochim. Acta 139, 411–433.

Solomon, S.C. et al., 2007. MESSENGER mission overview. Space Sci. Rev. 131, 3–39. http://dx.doi.org/10.1007/s11214-007-9247-6.

Stewart, S.T., Leinhardt, Z.M., Humayun, M., 2013. Giant impacts, volatile loss, and the K/Th ratios on the Moon, Earth, and Mercury. Lunar Planet. Sci. 44, abstract 2306.

Stockstill-Cahill, K.R. et al., 2012. Magnesium-rich crustal compositions on Mercury: Implications for magmatism from petrologic modeling. J. Geophys. Res. 117, E00L15. http://dx.doi.org/10.1029/2012JE004140.

Taylor, S.R., 1982. Planetary Science: A Lunar Perspective. Lunar and Planetary Institute, Houston, TX, 175 pp.
Taylor, G.J., Scott, E.R.D., 2003. Mercury. In: Davis, A.M. (Ed.), Meteorites, Comets, and Planets, Treatise on Geochemistry, vol. 1. Elsevier-Pergamon, Oxford, pp. 477–485.
Taylor, S.R., McLennan, S.M., 2008. Crusts: Their Composition Origin and Evolution. Cambridge Univ. Press, New York, p. 404 (ISBN:9780521142014).
Taylor, G.J. et al., 2010. K and Cl concentrations on the martian surface determined by the Mars Odyssey gamma-ray spectrometer: Implications for bulk halogen abundances in Mars. Geophys. Res. Lett. 37, L12204. http://dx.doi.org/10.1029/2010GL043528.
Thomas, R.J. et al., 2014. Long-lived explosive volcanism on Mercury. Geophys. Res. Lett. 41, 6084–6092. http://dx.doi.org/10.1002/2014GL061224.
Wadhwa, M., 2008. Redox conditions on small bodies, the Moon, and Mars. Rev. Mineral. Geochem. 68, 493–510.
Warren, P.H., 1988. KREEP: Major-element diversity, trace-element uniformity (almost). In: Taylor, G.J., Warren, P.H. (Eds.), Workshop on Moon in Transition: Apollo 14, KREEP, and evolved lunar rocks. Lunar and Planetary Institute, Houston, Tex., pp. 149–153.
Waters, L.S. (Ed.) 2002. MCNPX users' manual version 2.4.0, Rep. LA-CP-02-408, Los Alamos National Laboratory, Los Alamos, New Mex.
Webster, J.D., Kinzler, R.J., Mathez, E.A., 1999. Chloride and water solubility in basalt and andesite melts and implications for magmatic degassing. Geochim. Cosmochim. Acta 63, 729–738.
Weider, S.Z. et al., 2012. Chemical heterogeneity on Mercury's surface revealed by the MESSENGER X-Ray Spectrometer. J. Geophys. Res. 117, E00L05. http://dx.doi.org/10.1029/2012JE004153.
Weider, S.Z. et al., 2014. Variations in the abundance of iron on Mercury's surface from MESSENGER X-Ray Spectrometer observations. Icarus 235, 170–186. http://dx.doi.org/10.1016/icarus2014.03.002.
Weider, S.Z. et al., 2015. Evidence for geochemical terranes on Mercury: Global mapping of major elements with MESSENGER's X-Ray Spectrometer. Earth Planet. Sci. Lett. 416, 109–120.
Zolotov, M.Yu., 2011. On the chemistry of mantle and magmatic volatiles on Mercury. Icarus 212, 24–41. http://dx.doi.org/10.1016/icarus2010.12.014.
Zolotov, M.Yu. et al., 2013. The redox state, FeO content, and origin of sulfur-rich magmas on Mercury. J. Geophys. Res. Planets 118, 138–146. http://dx.doi.org/10.1029/2012JE004274.